Investigation of Integration Paths in the Spectral-Domain Analysis of Leaky Modes on Printed Circuit Lines

Francisco Mesa, *Member, IEEE,* and David R. Jackson, *Fellow, IEEE*

***Abstract*—The different integration paths that may arise in the spectral-domain analysis of leaky modes on open printed-circuit transmission lines such as microstrip are investigated. There are an infinite number of paths in the complex plane that may be used to construct leaky-mode solutions. Not all of the paths are valid mathematically. Among the mathematically valid ones, a certain subset correspond to paths that yield "physically valid" solutions. When tracking leaky-wave solutions as frequency changes, it is found that the propagation constants of the leaky modes may go through nonphysical "growing" regions where the attenuation constant is negative. These nonphysical regions may appear between physically valid frequency regions, implying that the leaky modes should be tracked in all frequency regions, including the nonphysical growing ones, in order to obtain the complete frequency dispersion behavior of the leaky mode. The migration of the leaky modes into these nonphysical growing regions gives rise to unconventional integration paths never seen before. Such paths must be used if the dispersion behavior of the leaky modes is to be plotted for all frequencies.**

***Index Terms*—Leaky modes, printed-circuit lines, spectral-domain techniques.**

I. Introduction

THE ISSUE of radiation and leakage on printed-circuit lines has received much attention [1]–[35] due to undesirable crosstalk and other spurious effects, as well as for potential applications to antennas and other devices [33], [34]. Leaky modes on open guiding structures such as microstrip (structures without a top cover) can leak into the surface-wave modes of the substrate structure, as well as into to free space [6]. The different nature of the leakage may be used to classify the leaky modes as surface-wave leaky modes and space + surface-wave leaky modes.

The analysis of leakage phenomena on printed-circuit lines is usually carried out by solving the electric-field integral equation (EFIE) in the spectral domain. In the spectral-domain integration, an arbitrariness is associated with the integration path used to define the inverse Fourier transform in the transverse wavenumber plane. In particular, the path may or may not detour around the various singularities of the spectral-domain Green's function (SDGF), including poles and branch points [12], [15], [16]. Among all the possible mathematical leaky-wave solutions arising from these different paths, only some of them are valid solutions of the boundary-value problem. Here, these solutions are called *mathematically valid* solutions. A subset of the mathematically valid solutions are also *physically valid* in the sense that such a leaky mode may appear as a significant part of the total current spectrum on the line when excited by a practical source, as shown in Fig. 1. In this paper, a comprehensive classification scheme is introduced to account for all possible paths that may be used to obtain leaky-mode solutions. It is briefly discussed when the paths correspond to mathematically valid solutions, and when they also correspond to physically valid solutions.

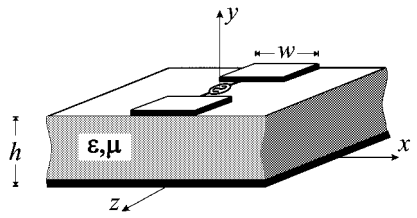

Fig. 1. Microstrip line on a lossless isotropic substrate, excited by a delta-gap voltage source.

The evolution of the leaky-mode solutions (and equivalently of their corresponding integration paths) as frequency changes is one of the main subjects of this investigation, and this is also aided by using the longitudinal wavenumber plane. It is shown that the continuous tracking of leaky-mode solutions may give rise to new integration paths never before seen. Although the solutions arising from such paths are not physically valid, the study of these paths is important since the corresponding solutions may be found in intermediate-frequency regions that are between the frequency ranges where the solutions are physically valid. The longitudinal wavenumber complex plane is found to be a very useful tool for examining the evolution of the leaky modes with respect to the frequency, since this evolution is equivalent to tracking the loci of the different leaky-mode solutions on the different sheets of a Riemann surface.

II. Classification of Integration Paths

This section will briefly overview the spectral-domain method as applied to leaky-mode solutions on printed-circuit structures, such as the microstrip line shown in Fig. 1. This will then be used to introduce the complex longitudinal wavenumber

Manuscript received March 29, 2001; revised December 20, 2001. This work was supported in part by the State of Texas Advanced Research and Technology Program. The work of F. Mesa was supported in part by the Comisión Interministerial de Ciencia y Tecnología, Spain under Project TIC98-0630.

F. Mesa is with the Department of Applied Physics I, University of Seville, 41012 Seville, Spain (e-mail: mesa@us.es).

D. R. Jackson is with the Department of Electrical and Computer Engineering, University of Houston, Houston, TX 77204-4005 USA.

Digital Object Identifier 10.1109/TMTT.2002.803433.

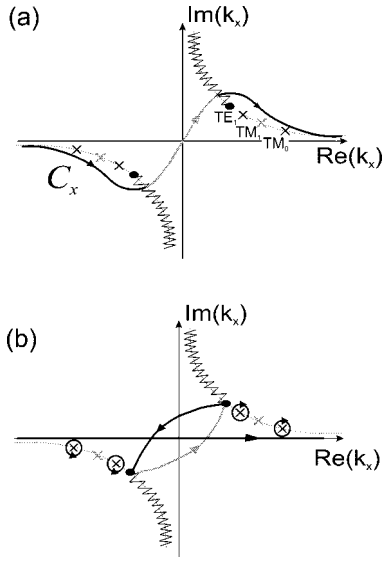

Fig. 2. (a) Possible integration path in the complex k_x-plane. For a given value of the propagation wavenumber k_z, this figure shows the location of the singularities of the SDGF. (b) The same integration path expressed as the sum of a real axis path plus a clockwise loop between the branch points, together with two circular paths around the proper poles.

(k_z)-plane, which is central to the later discussion of the integration paths in the transverse wavenumber (k_x)-plane.

In the spectral-domain analysis of propagation on infinite printed-circuit lines, the EFIE is typically solved by expanding the unknown current into basis functions and then applying Galerkin's method, yielding a determinantal dispersion equation of the form [26], [16]

$$F(k_z) \equiv \det\left[\int_{C_x} \Gamma_{mn}(k_x;\, k_z)\, dk_x\right] = 0 \qquad (1)$$

with

$$\Gamma_{mn}(k_x;\, k_z) = \tilde{\mathbf{J}}_m(-k_x) \cdot \overline{\mathbf{G}}(k_x;\, k_z) \cdot \tilde{\mathbf{J}}_n(k_x) \qquad (2)$$

being any of the entries of the Galerkin moment-method matrix, and $\tilde{\mathbf{J}}_n(k_x)$ being the Fourier transform of the nth basis function for the transverse shape of the surface current $\mathbf{J}(x)$ on the strip conductor.

In the transverse wavenumber k_x (integration) plane, branch points appear at $k_{xb} = \pm(k_0^2 - k_z^2)^{1/2}$, which create a two-sheeted Riemann surface for the k_x-plane. Poles appear at $k_{xp} = \pm(k_g^2 - k_z^2)^{1/2}$, where k_g is the wavenumber of a guided mode on the grounded dielectric substrate. (Poles on the top sheet of the k_x-plane correspond to surface-wave modes of the grounded dielectric substrate, while poles on the bottom sheet correspond to improper modes.) Various paths of integration are possible, corresponding to choices of detouring around the poles and branch points in various ways. For example, Fig. 2(a) shows a path that detours through the branch points and consequently lies partly on the bottom sheet. The part of the path on the top sheet detours above the poles corresponding to two surface-wave modes (the TM_0 and TE_1 modes). The part of the path on the bottom sheet detours above the pole corresponding to the TM_1 mode, which is assumed to be an improper real mode at this frequency (all other poles are ignored for simplicity). Fig. 2(b) shows an equivalent path, which will be used later in the proposed path classification scheme.

As explained in [23], for a fixed frequency, the function $F(k_z)$ defines a Riemann surface for the *longitudinal wavenumber* k_z-plane, with an infinite number of branch points. Each one of the sheets of the Riemann surface is related to a different C_x integration path in the complex k_x-plane. The differences among the integration paths come from the different singularities of the SDGF [25], [27] that may be detoured around by these integration paths. Specifically, it has been reported in [23] that, for an open line (without lateral or top enclosures) such as microstrip, the Riemann surface has the following three types of branch points.

1) The first type is a branch point at $k_z = \pm k_0$ (k_0 denotes the free-space wavenumber). There are an infinite number of sheets associated with this branch point. The zero sheet, by definition, is the one used to construct solutions that do not leak into space.
2) The second type is a branch point at $k_z = \pm k_{\mathrm{sw}}$, where k_{sw} is the wavenumber of a surface wave on the grounded dielectric layer. This type of branch point appears only on the even sheets of the k_0 branch point. There are two sheets associated with these branch points. The wavenumber of a bound-mode solution that does not leak into surface waves appears, by definition, on the top sheet of these branch points.
3) The third type is a branch point at $k_z = \pm k_{\mathrm{imp}}$, where k_{imp} is the wavenumber of a improper mode of the grounded dielectric layer, which includes both complex leaky modes and improper real modes (improper modes with a real propagation wavenumber). This type of branch point appears only on the odd sheets of the k_0 branch point. There are two sheets associated with these branch points.

For the bound mode of propagation on the microstrip line, the wavenumber k_z is purely real, and the solution does not leak either into space or into surface waves. The wavenumber for the bound mode solution lies on the sheet that is referred to as the "bound-mode sheet." This sheet, by definition, is the zero sheet of the k_0 branch point and the top sheet of the surface-wave branch points. For a wavenumber on this sheet, the path of integration in the k_x-plane is the real axis. A wavenumber on one of the other sheets corresponds to a leaky-mode solution that leaks into some combination of space and the surface waves of the grounded dielectric layer. More details on the branch points, including a thorough discussion of the properties mentioned above, may be found in [23].

In general, there are an infinite number of ways in which the integration path in the k_x-plane may be chosen since there are an infinite number of ways in which the integration path may detour around the various singularities of the SDGF. In order for a path to correspond to a *mathematically valid* solution, the corresponding wavenumber in the k_z-plane must be continuously trackable to a point on the bound-mode sheet (corresponding to a bound-mode solution). To illustrate, Fig. 3 shows how the path of integration in the k_x-plane evolves as the wavenumber k_z continuously moves from a point on the bound-mode sheet to various locations on the Riemann surface. In this figure, two

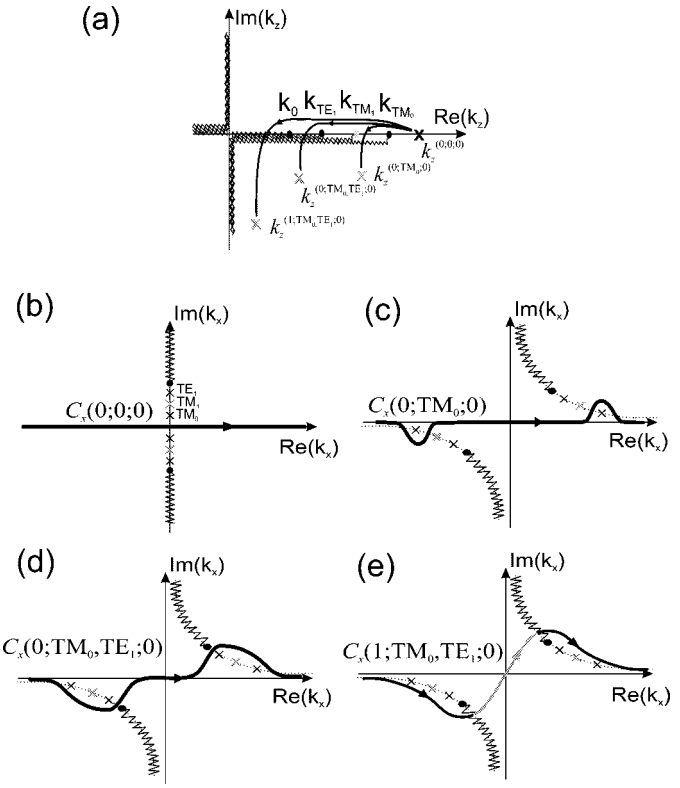

Fig. 3. (a) Possible excursions of the k_z wavenumber solution on the k_z Riemann surface, showing various paths that lead from the principle sheet [corresponding to an integration path $(0;0;0)$] to adjacent sheets. (b)–(e) The integration path C_x in the complex k_x-plane corresponding to the four k_z wavenumbers shown in (a) (denoted by $\times$).

surface-wave modes (TM_0 and TE_1) are assumed to be above cutoff, while the TM_1 mode is assumed to be an improper real mode below cutoff. (The TM_1 branch point and branch cut are shown shaded in gray since this branch cut is on a lower sheet of the k_0 branch point.) For simplicity, all other modes are ignored. The index notation used for the wavenumbers and the paths in the figure will be explained.

All the paths shown in Fig. 3 are mathematically valid, but they do not necessarily correspond to solutions that are physical. A physical mode is one that would appear in the spectrum for the current excited by a practical source, as shown in Fig. 1. The issue of physical validity was discussed in [23]. A mathematically valid solution is also a physical solution if it satisfies the path consistency condition (PCC), meaning that the phase constant of the mode that is obtained from a particular path of integration is *consistent* with the path. For example, a modal solution obtained from the path shown in Fig. 3(c) will be physical if the phase constant is less than that of the TM_0 surface wave, but greater than k_0 and also greater than the wavenumber of the TE_1 surface wave. More details may be found in [23].

Clearly, the paths can get rather complicated, when all possibilities are allowed (mathematically valid or not, and physically valid or not). A systematic way of classifying all the possible paths is desirable. To aid in the classification, it is first noted that an arbitrary C_x integration path can be expressed as the superposition of the following three parts [22], [23]:

1) path running along the entire real axis;
2) round-trip path (or loop) between the branch points of the SDGF, where each part of the loop is located on a different sheet;
3) set of paths encircling the proper or improper poles of the SDGF.

An example of this type of deformation is shown in Fig. 2(a) and (b), where (b) shows the different paths that constitute the original path in (a).

In light of the above consideration, the integration paths will be classified using three indexes, according to the following scheme.

1) The first index refers to the number of loops between the branch points, defined in the sense shown in Fig. 2(b) (counterclockwise if the proper part of the loop path is on top). For the example shown in Fig. 2(a), this index would be $+1$.
2) The second index is actually a list, indicating those proper surface-wave poles that are encircled, in the sense shown in Fig. 2(b). (The poles in the upper half-plane are encircled in the clockwise sense.) For the example shown in Fig. 2(a), this list would be (TM_0, TE_1). An encirclement in the counterclockwise sense would be denoted in this scheme by using a negative sign in front of the corresponding pole in the list. Multiple encirclements are denoted with an integer in front of the pole. For example, an index list that is ($2\mathrm{TM}_0$, TE_1) would indicate that the TM_0 pole is encircled twice in the clockwise sense. (The possibilities of negative or multiple encirclements do not correspond to mathematically valid paths, but such possibilities are allowed in the classification scheme to maintain generality.)
3) The third index is another list that indicates the improper poles (leaky-mode poles and improper-real mode poles) that are encircled. A positive encirclement is again defined by a clockwise integration around the pole for the pole that is in the upper half-plane. For an improper surface-wave pole with a real phase constant, this uniquely defines the integration path. For a complex leaky-mode pole, the situation is slightly more complicated since such a pole does not have to lie on the hyperbolic continuation of the branch-cut contour. To illustrate, consider the situation shown in Fig. 2(b). The leaky-mode pole in the first quadrant may lie to the right-hand side of the improper part of the loop path or to the left-hand side of it. If the pole lies to the right-hand side of this part of the loop path, and below the hyperbolic branch-cut contour, the classification scheme is the same as for the improper real modes. If the leaky-mode pole lies above the hyperbolic branch-cut contour, the classification scheme is also the same. If the leaky-mode pole lies to the left-hand side of the improper part of the loop path, and below the hyperbolic branch-cut contour, the integer in front of the name of the pole in the index is taken to be the number of clockwise residue loops around the pole minus one. For the example shown in Fig. 2(b), this third index list would be null since the improper pole is located to the right-hand side of the improper part of the loop path, with no residue paths around the pole.

To illustrate the above classification scheme, the integration path shown in Fig. 2(a) is denoted as $C_x(1;\mathrm{TM}_0, \mathrm{TE}_1;0)$. That is, C_x comprises the real axis, one counterclockwise loop between the branch points, circle paths around the poles on the top sheet of the k_x-plane associated with the wavenumbers of the TM_0 and TE_1 surface-wave modes of the substrate, each circled once in the clockwise sense, and no circle paths around the improper poles associated with the TM_1 (and the other) improper substrate modes. Every point on the k_z Riemann surface corresponds to a particular path of integration in the k_x-plane, which is designated using this classification scheme.

The above classification scheme was illustrated for the case when the poles and branch points are located in the first and third quadrants (as will be the case for physical leaky-mode solutions). For nonphysical growing leaky modes (with a negative attenuation constant), the poles and branch points will be located in the second and fourth quadrants. In this case, the path classification is obtained by allowing all the pole and branch point singularities in the k_x-plane to cross the imaginary axis, and then using the classification scheme as outlined above. This maintains the same path classification when the wavenumber k_z crosses the real axis in the k_z-plane without crossing any branch cuts.

The same classification scheme used for the paths can then be used to denote the particular sheet of the Riemann surface that the longitudinal wavenumber k_z is on. In Fig. 3, both the wavenumbers and the paths have been labeled using this classification scheme. In this scheme, the bound-mode sheet is denoted as $(0;0;0)$.

III. Discussion of Mode Splitting

One interesting aspect of modal evolution with frequency is the mode splitting that typically occurs on a lossless structure when the solution k_z merges with the conjugate solution k_z^*, resulting in a pair of improper-real solutions. Knowing when mode splitting will occur aids in the understanding of the frequency evolution of the k_z wavenumber.

A necessary condition for mode splitting to occur is that the solution k_z must approach the real axis in the k_z-plane. The wavenumber k_z^* is always a valid solution for a lossless structure and, hence, both k_z and k_z^* must approach the same set of coordinates as k_z approaches the real axis. However, this does not necessarily mean that the k_z and k_z^* solutions must evolve into a pair of improper real solutions when k_z approaches the real axis. This evolution will occur when the k_z and k_z^* solutions meet on the k_z Riemann surface. This, in turn, implies that the path of integration in the k_x-plane for the k_z solution must continuously evolve into the path of integration for the k_z^* solution as the wavenumber k_z crosses the real axis. The integration path for the k_z^* solution is simply the complex conjugate of the path used for the k_z solution. Hence, mode splitting will occur if the integration path changes into the corresponding conjugate path as k_z crosses the real axis on the Riemann surface.

To illustrate this, consider first a leaky-mode solution that leaks into only the TM_0 surface wave, corresponding to a path $(0;\mathrm{TM}_0;0)$. For such a leaky-mode solution with k_z located in the fourth quadrant [point #1 in Fig. 4(a)], the path of the integration is as shown in Fig. 4(b). If k_z at point #1 crosses

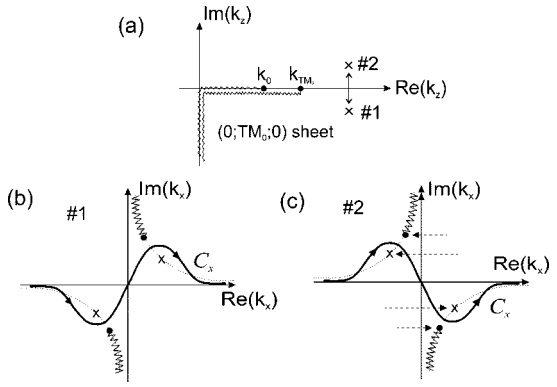

Fig. 4. (a) Trajectory in the k_z-plane, showing the wavenumber k_z crossing the real axis, moving from points #1 to #2. The wavenumber stays on the sheet that corresponds to the integration path $(0;\mathrm{TM}_0;0)$ in the k_x-plane. (b) and (c) Integration paths C_x in the k_x-plane corresponding to k_z wavenumbers at points #1 and #2 in the k_z-plane, respectively.

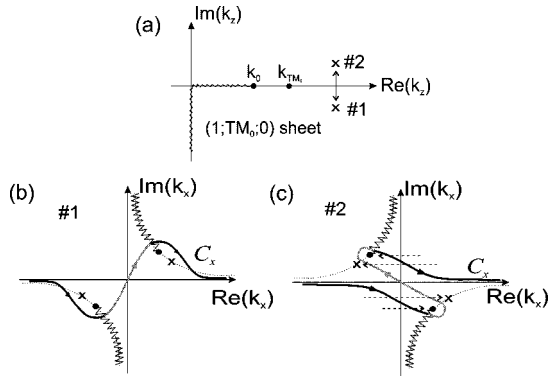

Fig. 5. (a) Trajectory in the k_z-plane, showing the wavenumber k_z crossing the real axis, moving from points #1 to #2. The wavenumber stays on the sheet that corresponds to the integration path $(1;\mathrm{TM}_0;0)$. (b) and (c) Integration paths C_x in the k_x-plane corresponding to k_z wavenumbers at points #1 and #2 in the k_z-plane, respectively.

the real axis to the right-hand side of the TM_0 branch point to reach point #2, the branch point and pole in the k_x-plane cross the imaginary axis, causing the path to evolve into the one shown in Fig. 4(c). This path is the conjugate path to the one shown in Fig. 4(b). Hence, if a TM_0 surface-wave leaky solution approaches the real k_z axis at a point to the right-hand side of the TM_0 branch point in the k_z-plane, mode splitting will occur. By similar reasoning, it can be shown that if the TM_0 surface-wave leaky solution approaches the real axis to the left-hand side of the TM_0 branch point, no mode splitting will occur.

Extending the reasoning, the general conclusion is that a leaky mode that leaks into a finite number of surface-wave modes will exhibit mode splitting if the k_z wavenumber approaches the real axis to the right-hand side of all the surface-wave branch points corresponding to the leakage.

Next, consider the case of a mode that leaks into both space and into the TM_0 surface wave, corresponding to the path $(1;\mathrm{TM}_0;0)$. The point labeled #1 in Fig. 5(a) is on the lower sheet of the k_0 branch point, and corresponds to the path shown in Fig. 5(b). If point #1 crosses the real k_z axis to the right-hand side of all the branch points, the path evolves into that shown in Fig. 5(c). This path is not the conjugate to the one shown in Fig. 5(b). Hence, a solution that leaks into space and

into the TM_0 surface wave will not encounter mode splitting as the solution approaches the real k_z axis to the right-hand side of the branch points. By following similar reasoning, it is also seen that a solution that leaks into both space and the TM_0 surface wave does not encounter mode splitting when the solution approaches the real axis to the left-hand side of any of the branch points. Hence, such a mode never encounters mode splitting.

In summary, mode splitting only occurs for a leaky-mode solution that leaks only into surface waves, and then only when the wavenumber k_z approaches the real axis to the right-hand side of all the corresponding branch points. This behavior will be observed in the results presented in Section IV.

IV. Evolution of Paths With Frequency

In the preceding sections, the integration paths in the k_x-plane were discussed, and it was shown how the path of integration continuously evolves as the wavenumber k_z moves on a Riemann surface (which may, for example, correspond to changing frequency). Also, a discussion of when mode splitting may occur as the wavenumber k_z approaches the real axis was given. These points will now be illustrated by showing results for a practical microstrip line. In addition to illustrating the above points, the results will show that a continuous tracking of the wavenumber with frequency may require that the wavenumber k_z crosses the real axis to enter a nonphysical "growing" region (the imaginary part of k_z is positive) during part of the frequency range. This leads to new and interesting paths of integration never seen before. Such paths must be used if the frequency behavior of the leaky mode is to be tracked continuously over the complete frequency range.

Results will be shown for a microstrip line on an isotropic substrate, having the parameters $h = 1.27$ mm, $w = 4$ mm and $\epsilon_r = 10.2$. This particular structure, with a high permittivity and a fairly wide strip, is chosen because it illustrates all of the aspects discussed previously, over a practical frequency range. Not every structure will exhibit all of these same effects over a given frequency range. Nevertheless, the general conclusions reached by studying this structure are expected to be valid for other structures, in the sense of demonstrating what types of path evolutions may occur as the frequency changes.

The normalized phase constants (β/k_0) for the fundamental bound mode and two leaky modes are shown in Fig. 6. This figure also shows the dispersion curves for the first two surface-wave modes of the grounded substrate (for frequencies below 19.2 GHz the TE_1 surface-wave mode is an improper-real mode). The light gray line corresponds to a leaky-mode solution that leaks into space and into the TM_0 surface-wave mode [obtained by using path $(1;\mathrm{TM}_0;0)$]. The dark gray line corresponds to a leaky-mode solution that leaks into only the TM_0 surface-wave mode [corresponding to a path $(0;\mathrm{TM}_0;0)$]. According to the PCC, the dominant bound mode, arising from path $(0;0;0)$, is physically valid for the entire frequency range. The $(0;\mathrm{TM}_0;0)$ solution is physically valid only at those frequencies where $k_0 < \beta < k_{\mathrm{TM}_0}$, i.e., approximately between 13–14 GHz and also between 18–26.2 GHz. Above 26.2 GHz, $\beta < k_{\mathrm{TE}_1}$, but the poles

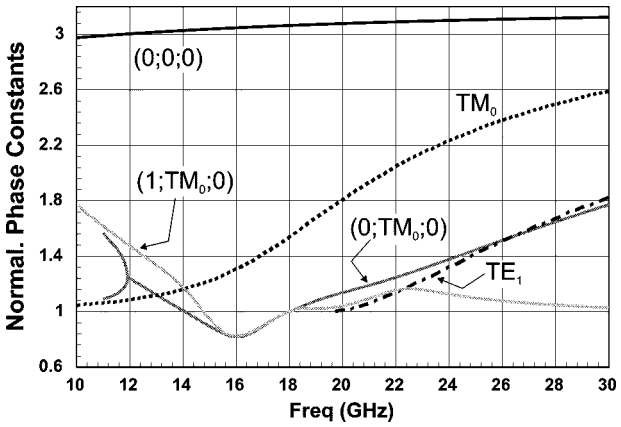

Fig. 6. Normalized phase constants (normalized by k_0) for the fundamental bound mode and two leaky modes of a microstrip with $h = 1.27$ mm, $w = 4$ mm, $\epsilon_r = 10.2$. One leaky mode leaks only into the TM_0 surface-wave mode of the grounded substrate. This mode is obtained by using the integration path $(0;\mathrm{TM}_0;0)$. The other leaky mode leaks into space as well as into the TM_0 surface wave. The corresponding integration path is $(1;\mathrm{TM}_0;0)$.

associated with the TE_1 surface-wave mode are not detoured around by the $(0;\mathrm{TM}_0;0)$ integration path in the k_x-plane; hence, this solution violates the PCC and, therefore, loses physical validity in this frequency region.

The only physical region for the $(1;\mathrm{TM}_0;0)$ solution is between 14.8–18 GHz, where $\beta < k_0$. It is observed that there is a frequency range (from 15.2 to 18 GHz) where the phase constants of the two leaky modes almost coincide. It might be assumed that this would be a region of strong coupling between the two leaky modes. However, the two leaky-wave solutions are on different sheets of the Riemann surface and, furthermore, only the $(1;\mathrm{TM}_0;0)$ solution is physically valid in this region. Hence, the usual mode coupling that occurs as the phase constants of two different modes approach each other is not found here.

The normalized phase and attenuation constants of the $(0;\mathrm{TM}_0;0)$ solution are shown in Fig. 7.

It is interesting to note in Fig. 7(b) that, between approximately 17–18 GHz, the attenuation constant α (with $k_z = \beta - j\alpha$) of this mode is negative. Clearly, a "growing" mode with a positive phase constant and a negative attenuation constant is not physical. Nevertheless, it is important to track the solution in this "anomalous" region because after this region, the $(0;\mathrm{TM}_0;0)$ solution is once again physically valid according to the PCC.

Insight into the frequency evolution of this mode is provided by examining the locus of the wavenumber solution in the complex k_z-plane, shown in Fig. 8. It is observed that there is a mode-splitting point at approximately 11.92 GHz when the wavenumbers of the two improper real modes meet on the real axis to the right-hand side of the k_{TM_0} branch point ($k_{\mathrm{TM}_0}/k_0 \simeq 1.09$ at this frequency). After the splitting point, a complex $(0;\mathrm{TM}_0;0)$ solution and its complex conjugate emerge perpendicularly. The solution in the fourth quadrant of the k_z-plane travels to the left-hand side of the quadrant until it crosses the branch cuts (not shown) on the real axis from both the k_0 and k_{TM_0} branch points at approximately 17 GHz. After this crossing, the solution goes to the first quadrant,

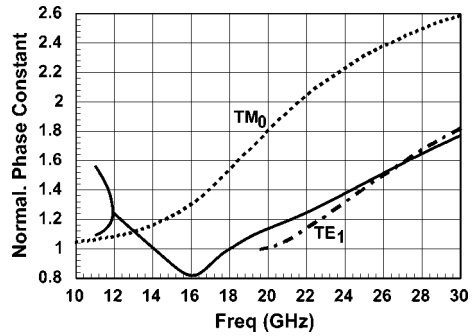

(a)

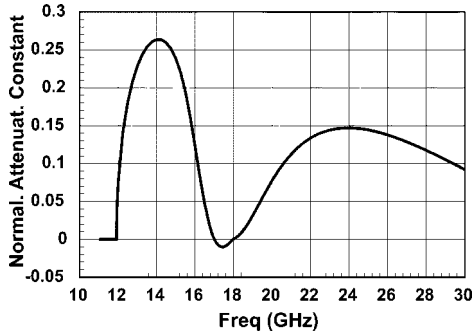

(b)

Fig. 7. (a) Normalized phase constant and (b) normalized attenuation constant for the surface-leaky mode in Fig. 6 obtained by using the integration path $(0; \mathrm{TM}_0; 0)$.

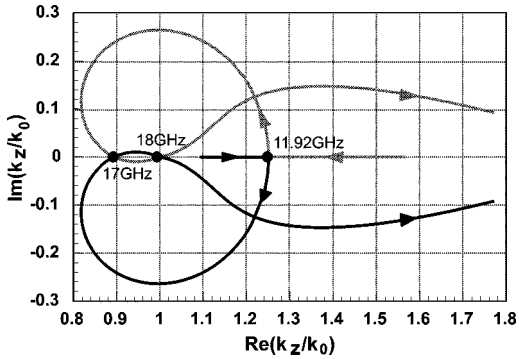

Fig. 8. Locus of the k_z wavenumber in the complex k_z-plane for the surface-wave leaky solution between 11–30 GHz. This figure shows the locus of both the complex leaky-mode solution (black line) and the complex conjugate solution (gray line) obtained by using the conjugate integration path.

entering the $(-1; -\mathrm{TM}_0; \mathrm{TE}_1)$ sheet of the Riemann surface, corresponding to the path $(-1; -\mathrm{TM}_0; \mathrm{TE}_1)$ in the k_x-plane. The path is shown in Fig. 9. (The designation for this path is obtained by first allowing the poles and branch points to cross the imaginary axis, and then examining the circle paths around the poles, as discussed previously in Section II.) The gray line in Fig. 8, corresponding to the locus of the complex conjugate solution, begins on the sheet $(0; \mathrm{TM}_0; 0)$ and crosses the branch cuts to enter the $(1; 0; 0)$ sheet in the fourth quadrant. Therefore, the loci of the original solution and its complex conjugate do not meet at 17 GHz, and there is no splitting point at this frequency. This behavior is as expected from the discussion in the previous section.

After an small excursion of the solutions on these sheets, they come back to the $(0; \mathrm{TM}_0; 0)$ sheet at approximately 18 GHz.

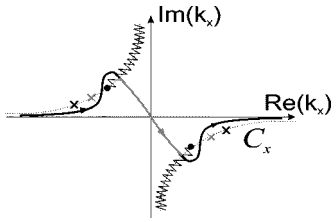

Fig. 9. Integration path C_x in the k_x-plane corresponding to a k_z wavenumber located in the first quadrant of the k_z-plane on the first upper sheet of the k_0 branch point [the sheet designated as $(-1; -\mathrm{TM}_0; \mathrm{TE}_1)$]. This path corresponds to the frequency range from 17 to 18 GHz in Fig. 8.

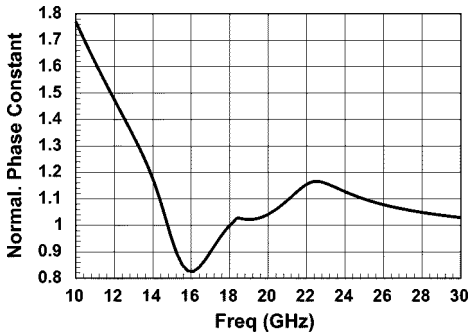

(a)

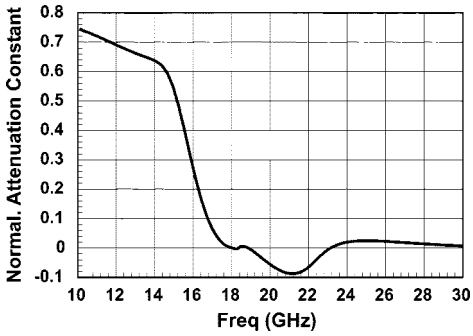

(b)

Fig. 10. (a) Normalized phase constant and (b) normalized attenuation constant for the space + surface-wave leaky mode in Fig. 6, obtained by using the integration path $(1; \mathrm{TM}_0; 0)$.

From this frequency up to 30 GHz, the solutions remain on this sheet.

The normalized phase and attenuation plots for the $(1; \mathrm{TM}_0; 0)$ solution are shown in Fig. 10. It is again observed in Fig. 10(b) that the attenuation constant takes negative values over the range shown; this time within two different frequency ranges between 18.035–18.375 GHz and 18.845–23.25 GHz. The locus of the solution in the k_z-plane is shown in Fig. 11 (the complex conjugate solution is not shown since, as discussed in the previous section, this solution never merges with the original solution to form mode splitting). Fig. 11 shows how the k_z wavenumber starts in the fourth quadrant on the sheet that corresponds to the $(1; \mathrm{TM}_0; 0)$ path and travels in this quadrant until it approaches the k_0 branch point. The corresponding integration path in the k_x-plane associated with this excursion in the k_z-plane is shown in Fig. 12(a). This figure also shows the following singularities of the SDGF in the k_x-plane: branch points associated with k_0, poles on the top (proper) sheet associated with the TM_0 surface-wave mode,

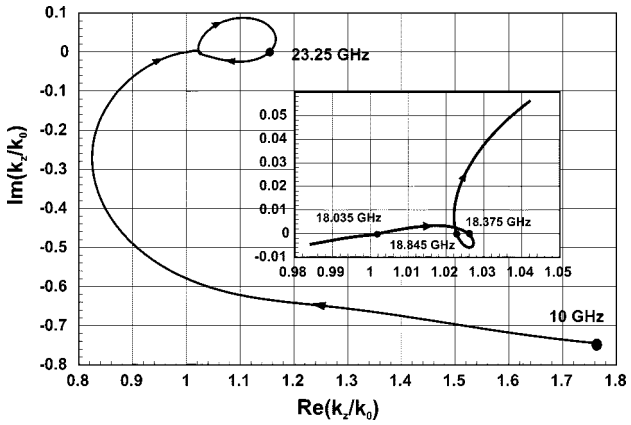

Fig. 11. Locus of the k_z wavenumber in the complex k_z-plane for the space + surface-wave leaky solution between 10–30 GHz.

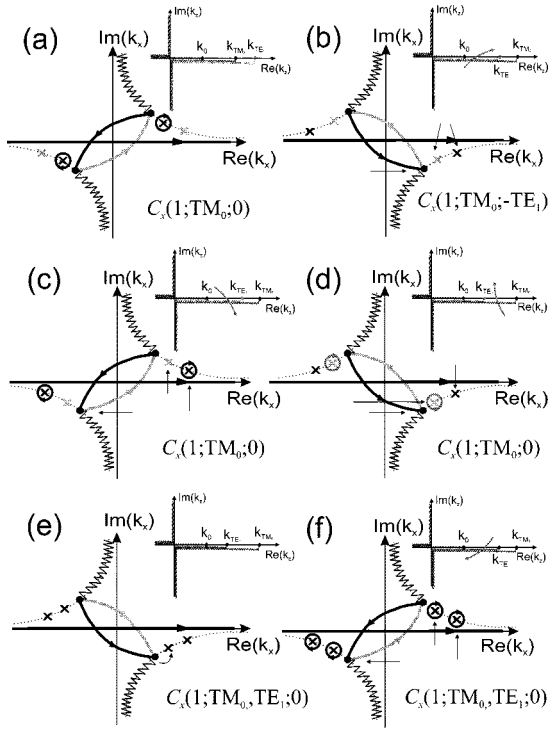

Fig. 12. Integration paths C_x in the k_x-plane that are used to track the space + surface-wave leaky solution in Fig. 11 in the following frequency regions. (a) Frequencies below 18.035 GHz. (b) Frequencies between 18.035–18.375 GHz. (c) Frequencies between 18.375–18.845 GHz. (d) Frequencies between 18.845–19.2 GHz. (e) Frequencies between 19.2–23.25 GHz. (f) Frequencies above 23.25 GHz.

and poles on the bottom (improper) sheet associated with the below-cutoff TE_1 surface-wave mode (which is actually an improper surface-wave mode).

The magnified inset of Fig. 11 shows how, after approaching the branch point at k_0, the wavenumber moves to the first quadrant (negative value of the attenuation constant) after crossing the real axis just to right-hand side of k_0 at approximately 18.035 GHz. (The inset sketch in Fig. 12(b) shows where the wavenumber crosses the real axis in relation to the branch points.) As the wavenumber crosses the real axis, it crosses the branch cut associated with the TE_1 improper surface-wave mode. No branch cuts associated with the TM_0 surface-wave mode are crossed because branch points associated with proper surface-wave modes do not appear on the lower sheet of the k_0 branch point, as mentioned previously [23]. After k_z crosses the real axis at 18.035 GHz, the branch points in the k_x-plane cross the imaginary axis, while the TM_0 poles on the top sheet and the TE_1 poles on the bottom sheet of the k_x-plane cross the real axis. After k_z crosses the real axis, the corresponding integration path in the k_x-plane is now that shown in Fig. 12(b), which is classified as path $(1;\mathrm{TM}_0;-\mathrm{TE}_1)$.

It should be noted that as frequency increases, the TE_1 surface-wave mode is approaching its cutoff frequency (19.2 GHz) and, therefore, the TE_1 poles in the k_x-plane come close to the branch points. This will result in an interesting transition in paths, as seen presently.

At 18.375 GHz, the k_z wavenumber again crosses the real axis and the TE_1 branch cut, and moves back to the fourth quadrant of the k_z-plane in the $(1;\mathrm{TM}_0;0)$ sheet, where it stays until it approaches in an upwards direction the real axis once again at approximately 18.845 GHz. Between 18.375–18.845 GHz the integration path is shown in Fig. 12(c). At 18.845 GHz, the TE_1 branch point on the real axis in the k_z-plane has moved sufficiently far to the left-hand side (toward the k_0 branch point) that it is now located on the real axis to the left-hand side of the point where the k_z wavenumber is approaching the real axis at 18.845 GHz. This implies that the wavenumber now does not cross this branch cut and, hence, the TE_1 improper poles cross the imaginary axis in the k_x-plane. Therefore, the path evolves from that shown in Fig. 12(c) to that shown in Fig. 12(d) as the frequency increases past 18.845 GHz. The path shown in Fig. 12(d) is classified as $(1;\mathrm{TM}_0;0)$.

The integration path in the k_x-plane remains the same until the cutoff frequency of the TE_1 surface-wave mode is reached (19.2 GHz), at which point the improper TE_1 poles in the k_x-plane coalesce with the branch points and then reemerge as proper surface-wave poles. As these poles reemerge to the proper sheet, they cross the improper part of the loop, adding other residue path contributions that null their previous improper residue paths. The path is then as shown in Fig. 12(e), which is classified as $(1;\mathrm{TM}_0,\ \mathrm{TE}_1;0)$.

At 23.25 GHz, the k_z solution crosses the real axis again, to the left-hand side of the TE_1 and TM_0 branch points (although their corresponding branch cuts are not crossed since they are not on the same sheet as the wavenumber). Both the TE_1 and TM_0 poles consequently cross the real axis, resulting in the path shown in Fig. 12(f), which remains classified as path $(1;\mathrm{TM}_0,\ \mathrm{TE}_1;0)$.

V. Conclusions

Many different integration paths are possible in the spectral-domain analysis of leaky-mode propagation on open printed-circuit structures such as microstrip. A classification scheme for characterizing these paths has been proposed here. Out of all the possible paths, a certain subset of these paths are mathematically valid in the sense that the resulting modal solution satisfies the boundary conditions at the strip conductor, as well as Maxwell's equations. A subset of these mathematically valid paths are also physically valid, yielding modal solutions that are physical in

the sense that such a leaky-mode solution would be physically present to an appreciable degree in the total spectrum of current that is produced on the line by a practical source.

The complex longitudinal wavenumber plane (the k_z-plane) provides insights about the mathematical and physical validity of the paths. In particular, a mathematically valid path is one that comes from a continuous evolution of the real-axis path (the one that is used to obtain bound-mode solutions) as the wavenumber k_z moves continuously on a Riemann surface. A path that is also physically valid is one that satisfies a PCC.

The concept of the Riemann surface for the longitudinal wavenumber k_z allows for other important conclusions regarding the frequency behavior of the wavenumber k_z. It was shown that mode splitting sometimes occurs when the wavenumber approaches the real axis (where a complex leaky solution meets a complex conjugate solution, and the two solutions split apart as two improper-real solutions). In other situations, mode splitting does not occur. The use of the k_z Riemann surface allows for a prediction of when mode splitting will occur. It was shown that mode splitting occurs when the complex leaky-mode solution and its complex conjugate solution meet on the Riemann surface.

Another interesting use of the k_z-plane is to provide insight into the evolution of the spectral-domain integration paths as frequency changes. It was shown that a continuous tracking of the wavenumber k_z may require that the wavenumber enter a nonphysical "growing" region of the complex plane, where the leaky-mode solution has a negative attenuation constant. Although such solutions are completely nonphysical, frequency regions exhibiting growing behavior may appear between physical frequency regions, making it necessary to track the solution through the nonphysical growing regions if the complete dispersion behavior of the line is to be obtained. The tracking of the solution into these nonphysical growing regions gives rise to new paths of integrations never before observed.

REFERENCES

[1] T. T. Wu, "Theory of the microstrip," *J. Appl. Phys.*, vol. 28, pp. 299–302, Mar. 1957.

[2] H. Ermest, "Guided modes and radiation characteristics of covered microstrip lines," *Arch. Elektron. Uebertrag.*, vol. 30, pp. 65–70, 1976.

[3] W. Menzel, "A new travelling-wave antenna in microstrip," *Arch. Elektron. Uebertrag.*, vol. 33, pp. 137–140, 1979.

[4] J. Boukamp and R. H. Jansen, "Spectral domain investigation of surface wave excitation and radiation by microstrip lines and microstrip disk resonator," in *Proc. 13th Eur. Microwave Conf.*, Sept. 1983, pp. 721–726.

[5] D. B. Rutledge, D. P. Neikirk, and D. P. Kasilingam, "Integrated circuit antennas," in *Infrared and Millimeter Waves*, K. J. Button, Ed. San Diego, CA: Academic, 1983, vol. 10, pp. 1–90.

[6] A. A. Oliner, "Leakage from higher modes on microstrip line with application to antennas," *Radio Sci.*, vol. 22, pp. 907–912, Nov. 1987.

[7] H. Shigesawa, M. Tsuji, and A. A. Oliner, "Conductor-backed slot line and coplanar waveguide: Dangers and full-wave analysis," in *Proc. IEEE MTT-S Int. Microwave Symp. Dig.*, June 1988, pp. 199–202.

[8] K. A. Michalski and D. Zheng, "Rigorous analysis of open microstrip lines of arbitrary cross section in bound and leaky regimes," *IEEE Trans. Microwave Theory Tech.*, vol. 37, pp. 2005–2010, Dec. 1989.

[9] T. Rozzi, F. Moglione, E. Marchionna, and M. Politi, "Hydrid modes, substrate leakage, and losses of slotline at millimeter-wave frequencies," *IEEE Trans. Microwave Theory Tech.*, vol. 38, pp. 1069–1078, Aug. 1990.

[10] D. S. Pathak, N. K. Das, and D. M. Pozar, "Dispersion characteristics of optically excited coplanar striplines: Comprehensive full-wave analysis," *IEEE Trans. Microwave Theory Tech.*, vol. 38, pp. 1719–1730, Nov. 1990.

[11] N. K. Das and D. M. Pozar, "Full-wave spectral-domain computation of material, radiation, and guided wave losses in infinite multilayered printed transmission lines," *IEEE Trans. Microwave Theory Tech.*, vol. 39, pp. 54–63, Jan. 1991.

[12] H. Shigesawa, M. Tsuji, and A. A. Oliner, "Dominant mode power leakage from printed-circuit waveguide," *Radio Sci.*, vol. 26, pp. 559–564, Mar.–Apr. 1991.

[13] J.-Y. Ke, I.-S. Tsai, and C. H. Chen, "Dispersion and leakage characteristics of coplanar waveguides," *IEEE Trans. Microwave Theory Tech.*, vol. 40, pp. 1970–1973, Oct. 1992.

[14] J. M. Grimm and P. P. Nyquist, "Spectral analysis considerations relevant to radiation and leaky modes of open-boundary microstrip transmission line," *IEEE Trans. Microwave Theory Tech.*, vol. 41, pp. 150–153, Jan. 1993.

[15] D. Nghiem, J. T. Williams, D. R. Jackson, and A. A. Oliner, "Proper and improper dominant mode solutions for stripline with an airgap," *Radio Sci.*, vol. 28, no. 6, pp. 1163–1180, Nov.–Dec. 1993.

[16] F. Mesa and R. Marqués, "Integral representation of spatial Green's function and spectral domain analysis of leaky covered strip-like lines," *IEEE Trans. Microwave Theory Tech.*, vol. 43, pp. 828–837, Apr. 1995.

[17] J. L. Cina and L. Carin, "Mode conversion and leaky-wave excitation at open-end coupled-microstrip discontinuities," *IEEE Trans. Microwave Theory Tech.*, vol. 43, pp. 2066–2071, Sept. 1995.

[18] D. Nghiem, J. T. Williams, D. R. Jackson, and A. A. Oliner, "Leakage of the dominant mode on stripline with a small air gap," *IEEE Trans. Microwave Theory Tech.*, vol. 43, pp. 2549–2556, Nov. 1995.

[19] F. Mesa and R. Marqués, "Power based considerations on the spectral domain analysis of leaky waves in covered strip-like transmission lines," *Proc. Inst. Elect. Eng.*, vol. 143, pp. 25–30, Jan. 1996.

[20] N. K. Das, "Power leakage, characteristic impedance and leakage-transition behavior of finite-length stub section of leaky printed transmission lines," *IEEE Trans. Microwave Theory Tech.*, vol. 44, pp. 526–536, Apr. 1996.

[21] D. Nghiem, J. T. Williams, D. R. Jackson, and A. A. Oliner, "Existence of a leaky dominant mode on microstrip line with an isotropic substrate: Theory and measurements," *IEEE Trans. Microwave Theory Tech.*, vol. 44, pp. 1710–1715, Oct. 1996.

[22] C. Di Nallo, F. Mesa, and D. R. Jackson, "Excitation of leaky modes on multilayer stripline structures," *IEEE Trans. Microwave Theory Tech.*, vol. 46, pp. 1062–1071, Aug. 1998.

[23] F. Mesa, C. Di Nallo, and D. R. Jackson, "The theory of surface-wave and space-wave leaky modes excitation on microstrip lines," *IEEE Trans. Microwave Theory Tech.*, vol. 47, pp. 207–215, Feb. 1999.

[24] P. Morse and H. Feshbach, *Methods of Theoretical Physics*. New York: McGraw-Hill, 1953.

[25] R. E. Collin, *Field Theory of Guided Waves*, 2nd ed. New York: IEEE Press, 1991.

[26] T. Itoh, *Numerical Techniques for Microwave and Millimeter-Wave Passive Structures*. New York: Wiley, 1989.

[27] R. Marqués and F. Mesa, "Spectral domain analysis of higher order leaky modes in microstrip lines: A new spectral-gap effect," *J. Electromagn. Waves Applicat.*, vol. 11, pp. 1367–1384, Nov. 1997.

[28] D. P. Nyquist and D. J. Infante, "Discrete higher-order leaky-wave modes and the continuous spectrum of stripline," *IEICE Trans. Commun.*, vol. E78-C, pp. 1331–1338, Oct. 1995.

[29] D. R. Jackson, F. Mesa, M. J. Freire, D. P. Nyquist, and C. Di Nallo, "An excitation theory for bound modes, leaky modes, and residual-wave currents on stripline structures," *Radio Sci.*, vol. 35, no. 2, pp. 495–510, Mar.–Apr. 2000.

[30] H. Shigesawa, M. Tsuji, and A. A. Oliner, "The nature of the spectral-gap between bound and leaky solution when dielectric loss is present in printed-circuit lines," *Radio Sci.*, vol. 28, no. 6, pp. 1235–1243, Nov.–Dec. 1993.

[31] ——, "A simultaneous propagation of bound and leaky dominant modes on printed-circuit lines: A new general effect," *IEEE Trans. Microwave Theory Tech.*, vol. 43, pp. 3007–3019, Dec. 1995.

[32] G. W. Hanson and A. D. Yakolev, "An analysis of the leaky-wave dispersion phenomena in the vicinity of cutoff using complex frequency plane singularities," *Radio Sci.*, vol. 33, no. 6, pp. 803–819, July–Aug. 1998.

[33] G.-J. Chou and C.-K. C. Tzuang, "Oscillator-type active-integrated antenna: The leaky mode approach," *IEEE Trans. Microwave Theory Tech.*, vol. 44, pp. 2265–2272, Dec. 1996.

[34] Y.-D. Lin and J.-W. Sheen, "Mode distinction and radiation-efficiency analysis of planar leaky-wave line source," *IEEE Trans. Microwave Theory Tech.*, vol. 45, pp. 1672–1680, Oct. 1997.
[35] F. Mesa and M. Horno, "Computation of proper and improper modes in multilayered bianisotropic waveguides," *IEEE Trans. Microwave Theory Tech.*, vol. 43, pp. 233–236, Jan. 1995.

Francisco Mesa (M'94) was born in Cádiz, Spain, in April 1965. He received the Licenciado and Doctor degrees from the University of Seville, Seville, Spain, in 1989 and 1991, respectively, both in physics.

He is currently an Associate Professor in the Department of Applied Physics I, University of Seville. His research interest focuses on electromagnetic propagation/radiation in planar lines with general anisotropic materials.

David R. Jackson (S'83–M'84–SM'95–F'99) was born in St. Louis, MO, on March 28, 1957. He received the B.S.E.E. and M.S.E.E. degrees from the University of Missouri, Columbia, in 1979 and 1981, respectively, and the Ph.D. degree in electrical engineering from the University of California at Los Angeles (UCLA), in 1985.

From 1985 to 1991, he was an Assistant Professor in the Department of Electrical and Computer Engineering, University of Houston, Houston, TX. From 1991 to 1998, he was an Associate Professor in the same department and, since 1998, he has been a Professor. His current research interests include microstrip antennas and circuits, leaky-wave antennas, leakage and radiation effects in microwave integrated circuits, periodic structures, and bioelectromagnetics. He is an Associate Editor for the *International Journal of RF and Microwave Computer-Aided Engineering*. He was an Associate Editor for *Radio Science*.

Dr. Jackson is the chapter activities coordinator for the IEEE Antennas and Propagation Society (IEEE AP-S) and the chair of the Technical Activities Committee for URSI, U.S. Commission B. He is also a distinguished lecturer for the IEEE AP-S Society. He was an associate editor for the IEEE TRANSACTIONS ON ANTENNAS AND PROPAGATION. He is a past member of the IEEE AP-S Administrative Committee (AdCom).